

The dependence of the sublimation temperature of the soot particles formed in the flames on their size and structure

© E.V. Gurentsov, A.V. Drakon, A.V. Eremin, R.N. Kolotushkin, E.Yu. Mikheyeva

Joint Institute for High Temperatures, Russian Academy of Sciences, Moscow, Russia
e-mail: gurentsov@ihed.ras.ru

Received July 7, 2021

Revised September 24, 2021

Accepted October 4, 2021

In this paper, the dependence of the sublimation temperature of soot particles synthesized during the combustion of various hydrocarbons, depending on their size and structure, is obtained. The experimental approach is based on the analysis of the thermal radiation of particles heated to the sublimation temperature by a nanosecond laser pulse. The sublimation temperature of soot particles was measured using the two-color pyrometry method. In this paper, it is proposed to use the average size of primary particles to compare data in different flames. It is established, that the sublimation temperature of soot particles depends mainly on the stage of their formation, which is characterized by an increase in average size. It is shown, that with an increase in the average particle size from 12 to 23 nm, their sublimation temperature increases significantly from 2700 to 4500 K. This reflects a significant difference in the thermodynamic and optical properties of the so-called "young" and "mature" soot particles, which must be taken into account when developing methods of soot diagnostics and in the thermo-physical analysis of combustion and pyrolysis processes with the formation of soot.

Keywords: flames, soot particles, sublimation temperature, structure of soot particles, transmission electron microscopy, laser-induced incandescence.

DOI: 10.21883/TP.2022.01.52533.206-21

Introduction

Soot is amorphous nanocarbon consisting of „primary“ spherical carbon nanoparticles combined into aggregates of a fractal structure. Each primary particle 5–50 nm in size consists of chaotically combined crystallites, which, in turn, have the form of stacks of graphene planes with a size on the order of 1 nm [1,2]. The general mechanism of soot formation was detailed in [3]. The process of formation of soot in combustion and pyrolysis of hydrocarbons may be divided into three stages. At the first stage, hydrocarbons undergo pyrolysis under the influence of high temperature (up to 2000°C). This results in the formation of smaller intermediate products for the first aromatic ring with subsequent addition of other aromatic and alkyl compounds and the formation of polycyclic aromatic hydrocarbons (PAHs) with 25–40 carbon atoms [4,5]. According to the most widespread theory, the hydrogen-abstraction/acetylene (C₂H₂)-addition (HACA) pathway is the dominant one for the formation of PAHs [6]. At the second stage, precursors of soot particles form. A universally accepted mechanism of formation of soot precursors has not been formulated yet. It is known that precursors are very small particles with a maximum diameter of 1–3 nm [4,7]. One hypothesis of formation of precursors is that large polyaromatic molecules combine into stacks (the so-called crystallites) [4]. The stage of formation of precursors defines the key parameters of a soot aerosol. At the third stage, soot particles grow from precursors in the process of agglomeration and due to heterogeneous reactions on their surface [3].

The knowledge of thermodynamic properties of soot particles is needed to develop soot diagnostics methods and for heat-exchange calculations for combustion chambers, boilers, and other equipment the operation of which involves sooting. It is hard to analyze the thermodynamic properties of soot particles theoretically, since their internal structure is considerably nonuniform and may vary from fully amorphous with disordered graphene planes (up to 2–3 nm in size) to partially crystalline with graphene layers forming the so-called crystallites (stacks of several parallel planes with an interplanar distance exceeding somewhat the corresponding distance in graphite (0.335 nm) [8]). Crystallites with different degrees of ordering form spherical primary soot particles with a mean size of 10–30 nm. Thus, experimental methods are crucial for the study of thermodynamic properties of different soot particles.

It was demonstrated in [9–12] that the optical properties of soot particles vary considerably over the flame height. The height above the burner face in flames is an equivalent of the reaction time in constant-volume reactors such as a shock tube [13]. It is natural to assume that the thermodynamic properties of soot particles formed in flames also depend on the stage of their formation and on the type of hydrocarbon fuel used.

The sublimation temperature is an essential thermodynamic property of soot particles. It allows one to determine the entire complex of thermodynamic properties [14]. Pulsed laser radiation with a wavelength of 1064 nm is typically used to heat soot particles to the sublimation temperature. Thermal radiation (incandescence) produced

under pulsed laser treatment is much more intense than the radiation of flame and may be used to determine the current temperature of soot particles [15,16]. The sublimation temperature is determined by measuring the maximum temperature of laser-heated soot particles as function of the energy density of laser radiation. When the sublimation threshold of soot particles is reached at a laser energy density of $0.1\text{--}0.2\text{ J/cm}^2$ (with a pulse duration of $5\text{--}10\text{ ns}$ at a wavelength of 1064 nm), the maximum heating temperature of particles ceases to increase and reaches a plateau, thus providing evidence of a phase transition. The sublimation of nanoparticles subjected to laser heating was also detected in the study of pyrolysis of hydrocarbons in a shock tube by laser extinction [13,17,18]. Thus, laser-induced incandescence (LII) is a promising technique for the study of thermophysical properties of nanoparticles. The sublimation temperatures of soot particles measured to date using the LII method were reviewed in [19]. The studies of carbon nanoparticles synthesized in the process of pyrolysis of hydrocarbons in a shock tube [13,17] revealed that the sublimation temperature increases from 2700 to 3300 K as particles grow in size from 2 to 12 nm . In addition, the sublimation temperature depended strongly on the post-shock temperature.

In contrast to shock-tube experiments in flames, studies of the sublimation temperature of soot particles were mostly conducted with reference to the flame height, and the particle size was not always measured.

The variety of thermodynamic and optical properties of soot particles is evidently related to the specifics of their internal structure [20]. In the past decade, soot particles of various structures have been studied by high-resolution transmission electronic microscopy (HR-TEM), which provides an opportunity to determine the structural parameters of the „framework“ of soot particles that is made of separate fringes (the end faces of graphene planes). Among these parameters are the length of a graphene plane, its curvature, and the interplanar distance [21].

The aim of the present study is to measure the sublimation temperature of soot particles in ethylene/air, acetylene/air, and propylene/air flames as function of their sizes and determine how the obtained dependences are correlated with parameters of the internal structure and the size of particles.

1. Research methods

1.1. Burner

Experiments in flames of premixed gases were conducted using a standard flat-flame McKenna burner (Holthuis & Associates) with a porous bronze surface and a diameter of 62 mm (Fig. 1). A brass disk 60 mm in diameter and 20 mm in thickness located at a height of 23 mm (or 30 mm for the propylene/air flame) above the burner face was used to stabilize the flame. The burner had an external ring gas-supply circuit for additional flame

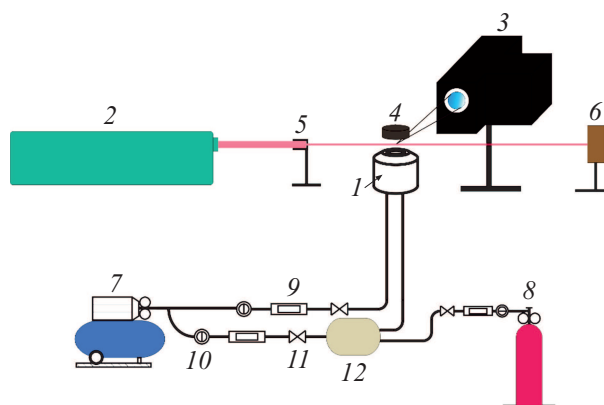


Figure 1. Diagram of the experimental setup based on a burner for flat premixed flames: 1 — burner, 2 — Nd:YAG laser, 3 — device for measuring LII signals with two photomultipliers fitted with filters centered at 450 and 670 nm , 4 — flame stabilizer, 5 — aperture, 6 — laser energy meter, 7 — air compressor, 8 — hydrocarbon vessel, 9 — flow meters, 10 — filters, 11 — valves, and 12 — mixing chamber.

stabilization. In the present study, air from a compressor was used for this purpose. When the fuel/oxidizer ratio is above the stoichiometric one, a fraction of fuel is spent on heating the gas, and soot particles form in the process of pyrolysis of the remaining fuel. Within the approximation of a one-dimensional structure of a flat flame, the molar fractions of substances and the temperature depend only on the height above the burner face. In the present experiments, ethylene/air flames: $\text{C}_2\text{H}_4\text{--}14.08\%$; $\text{O}_2\text{--}18.05\%$; $\text{N}_2\text{--}67.87\%$ with the $\text{C/O}=0.78$ ratio; acetylene/air flames: $\text{C}_2\text{H}_2\text{--}13.28\%$; $\text{O}_2\text{--}18.45\%$; $\text{N}_2\text{--}68.27\%$ with the $\text{C/O}=0.72$ ratio; and propylene/air flames: $\text{C}_3\text{H}_6\text{--}11.2\%$; $\text{O}_2\text{--}18.6\%$; $\text{N}_2\text{--}70.2\%$ with the $\text{C/O}=0.9$ ratio were studied. The flow rates of gases were monitored with RRG-10 (Eltochpribor) mass flow controllers. Type B platinum-rhodium thermocouples with a wire diameter of $45\text{ }\mu\text{m}$ and a junction diameter of $70\text{ }\mu\text{m}$ were used to measure the temperature over the flame height. The actual gas temperature was estimated with convective and radiation heat losses in the flame and the deposition of soot particles on the thermocouple junction taken into account in accordance with the procedure outlined in [22]. An LQ-215 (SOLAR Laser Systems) Nd:YAG laser operating at a wavelength of 1064 nm was used to heat soot particles. LII signals were detected at two wavelengths with the use of two H6780-20 photomultipliers with a rise time of 0.78 ns . Modules were fitted with narrowband filters centered at 450 and 670 nm . Signals were recorded by a LeCroy WavePro 7100 oscilloscope with a bandwidth of 1 GHz .

1.2. Measurement of the sublimation temperature of soot particles

The maximum temperature of laser-heated soot particles was measured by two-color pyrometry. The maximum

amplitude of LII signals was measured for this purpose at two wavelengths within the visible range (450 and 670 nm). Figure 2 shows the temporal evolution of example LII signals recorded in the acetylene/air flame at a height of 17 mm. Within the duration of a single laser pulse (6 ns), the LII signal reaches its maximum due to an increase in the particle temperature. When the pulse ends, the signal fades as the temperature decreases.

Since the spectral density of emission of soot particles follows the Planck's law, their current temperature may be written as in [23]

$$T_p = \frac{hc}{k_B} \times \frac{(1/\lambda_2 - 1/\lambda_1)}{\ln(S_1 S_{BB2} \varepsilon(\lambda_2) / S_2 S_{BB1} \varepsilon(\lambda_1)) + hc / k_B T_{BB} (1/\lambda_2 - 1/\lambda_1)}, \quad (1)$$

where h is the Planck's constant, c is the speed of light in vacuum, k_B is the Boltzmann constant, S_1, S_2 are the maxima of amplitudes of LII signals at wavelengths λ_1 and λ_2 , S_{BB1} and S_{BB2} are the amplitudes of signals from a radiation source with a known temperature, T_{BB} is the source temperature, and $\varepsilon(\lambda_{1,2})$ are the emissivities of particles at observation wavelengths λ_1 and λ_2 . The following expression is used to determine the emissivity of nanoparticles in the Rayleigh limit (the particles are much smaller than the wavelength) [24]:

$$\varepsilon(\lambda) = \frac{4\pi d_p E(m)}{\lambda}. \quad (2)$$

Here, d_p is the mean size of primary soot particles and $E(m)$ is the function of the refractive index ($m = n - ik$) of soot particles:

$$E(m) = -\text{Im}\left(\frac{m^2 - 1}{m^2 + 2}\right) = \frac{6nk}{(n^2 - k^2 + 2)^2 + 4n^2k^2}. \quad (3)$$

The ratio of emissivities of soot particles at wavelengths of 450 and 670 nm was determined based on

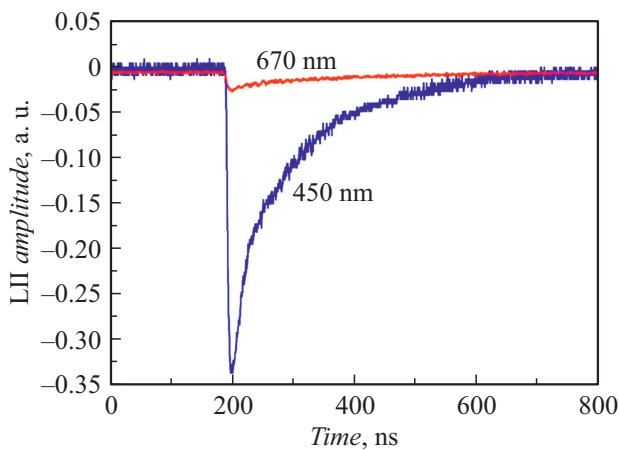


Figure 2. Temporal evolution of example LII signals recorded in the acetylene/air flame at a height of 17 mm and a laser radiation energy density of 0.13 J/cm².

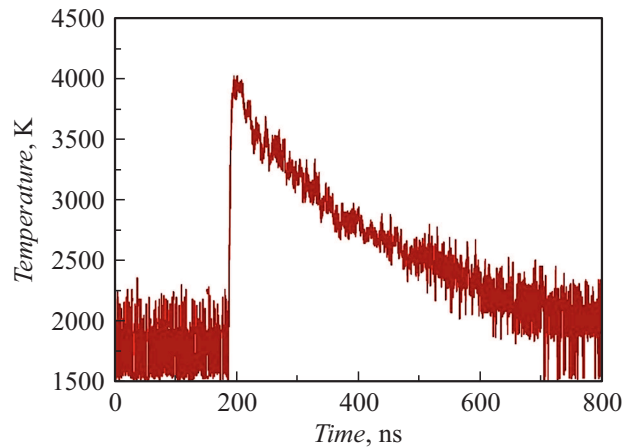


Figure 3. Example temporal profile of the temperature of laser-heated soot particles synthesized in the acetylene/air flame at a height of 17 mm at a laser radiation energy density of 0.13 J/cm².

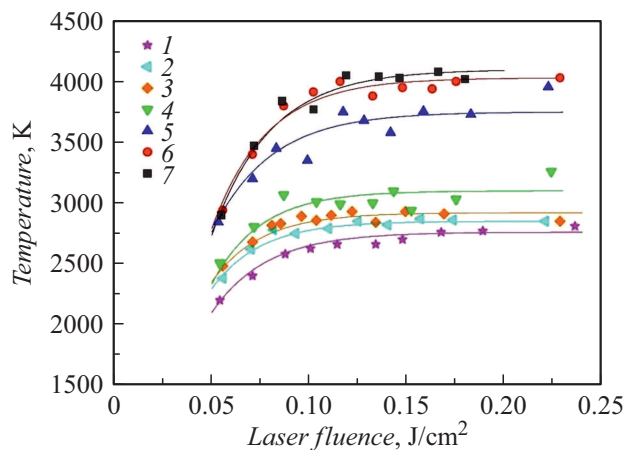


Figure 4. Dependences of the maximum temperatures of laser heating of soot particles synthesized in the acetylene/air flame (measured by two-color pyrometry) on the laser energy density. Height above the burner face: 1 – 5, 2 – 7, 3 – 10, 4 – 13, 5 – 15, 6 – 17, 7 – 20 mm. Solid curves represent the results of approximation.

the $E(m, 1064)/E(m, 532)$ ratios measured in [11,12] for wavelengths of 1064 and 532 nm in the corresponding flames at each flame height. It was assumed that $E(m)$ depends linearly on the wavelength. An example temporal profile of the temperature of laser-heated soot particles synthesized in the acetylene/air flame at a height of 17 mm is presented in Fig. 3. It can be seen that the maximum temperature of particles subjected to laser heating in these conditions is 4000 K, which is considerably higher than the flame temperature measured with the thermocouple (1500–1800 K).

Figure 4 presents the dependences of the maximum temperatures of laser heating of nanoparticles synthesized in the acetylene/air flame (measured by two-color pyrometry) on the laser energy density. It can be seen that the maximum

temperatures of laser-heated soot particles increase as the laser energy density grows from 0.05 to 0.1 J/cm², since the energy absorbed by particles also increases. At laser energy densities below 0.05 J/cm², the low signal-to-noise ratio precluded us from measuring the temperature correctly by the two-color method. The maximum temperatures of soot particles did not change as the laser energy density grew further above 0.1 J/cm², which was interpreted as a phase transition (soot sublimation) occurring at this temperature. This interpretation was confirmed by the measurement of a sharp reduction in the volume fraction of the condensed phase at the moment of laser irradiation in a shock-tube reactor [13,17]. It can be seen from Fig. 4 that the sublimation temperature depends on the height above the burner face, which corresponds to different stages of growth of soot particles or different reaction times. The sublimation temperature at a height of 5–13 mm is significantly lower than the sublimation temperature of soot formed at a height of 15–20 mm. This difference may be attributed to the presence of „young“ and „mature“ soot particles, which also differ in their optical and thermophysical properties, at these heights [25–28]. The error of the sublimation temperature of soot particles determined this way is estimated at ±4%.

1.3. Transmission electron microscopy

Transmission electron microscopy (TEM) was used to analyze the mean size and structure of soot particles. Particle samples were placed on copper grids for electron microscopy covered with a microperforated carbon monolayer. Grids were secured in a holder with a mechanical pneumatic actuator to sample soot by introducing them into the flame for a short time at a certain height above the burner face. The exposure time of a grid in the flame was 100 ms. Particle samples were analyzed using a FEI Osiris transmission electron microscope with an accelerating voltage of 200 kV at the federal research center „Crystallography and Photonics“ of the Russian Academy of Sciences.

Low-resolution photomicrographs were used to plot the size distributions of primary soot particles, which were produced in the three studied flames, with height above the burner face. More than a thousand measurements of primary particles were used to plot each distribution. The mean sizes of particles were determined by approximating the obtained distribution with a log-normal function. Figure 5 presents the dependences of the mean sizes of soot particles on the flame height. At lower heights, the amount of accumulated material was not sufficient for TEM analysis.

Figure 5 allows one to determine the regions of sootless and sooting flame in the studied conditions. The smallest sizes of soot particles corresponded to such heights above the burner face below which soot samples could not be obtained with a discretization of 1 mm in height („minimum“ heights). The sootless region, which is blue in color, for ethylene/air, acetylene/air, and propylene/air flames occupied the height intervals of 0–6, 0–4, and 0–12 mm,

respectively. Sooting regions (yellow in color) were located at greater heights. Thus, the size of soot particles increases sharply at a height of 6–7, 4–5, and 12–13 mm for ethylene/air, acetylene/air, and propylene/air flames, respectively. At greater heights, the sizes of primary soot particles vary more smoothly with height and reach approximately constant values, beyond which only aggregates grow in size.

Parameters of the internal structure of primary soot particles were determined using high-resolution photomicrographs. The algorithm for analysis of high-resolution TEM images was detailed earlier in [29,30]. Images were processed in ImageJ. The processing algorithm included the stage of highlighting a characteristic region of the soot structure on a high-resolution TEM image. The chosen image regions were saved as 8-bit grayscale images 512 × 512 pixels in size. Unprocessed digitized images were subjected to the fast Fourier transform and filtered with the use of circular masks with a size of 0.335 nm (distance between graphite layers) and 0.7 nm (distance at which the Van der Waals forces acting between two layers may be considered insignificant). After the inverse transform, fine image details were ignored. The filtered image was converted into a binary black-and-white one by setting a threshold brightness value for the phase boundary. The obtained image was skeletonized by compressing dark regions till they shrink to a pixel in width. Each individual fringe is regarded as an independent object (the end face of a graphene plane). Fringes shorter than 0.25 nm were excluded, since this value corresponds to the size of a single aromatic ring. Skeletonized images allowed us to perform statistical measurements of the length, the curvature (ratio of the fringe length to the straight distance between the ends of a fringe), and the interplanar distance between parallel fringe within the structure of soot particles. Figure 6 presents an example of conversion of a high-resolution TEM image into the structure of the carbon framework of a soot particle sampled in the propylene/air flame at a

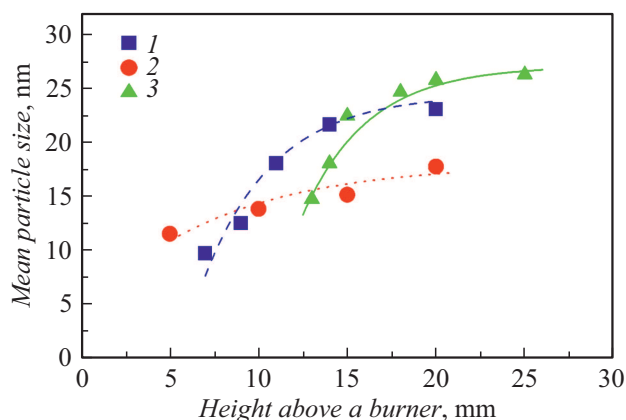


Figure 5. Variation of the mean sizes of soot particles with height for ethylene/air (1), acetylene/air (2), and propylene/air (3) flames. Curves represent the results of least-squares approximation of the experimental data.

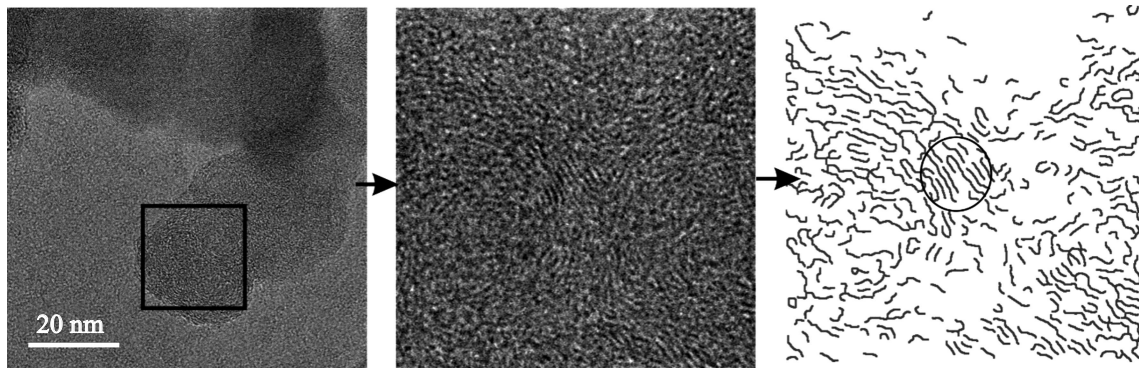


Figure 6. Conversion of a high-resolution image into a skeletonized structure of a soot particle containing crystallites. Sampling was performed at a height of 20 mm in the propylene/air flame.

height of 20 mm that corresponds to the final stage of soot formation. The region containing crystallites is circled.

2. Results and discussion

Figure 7 shows the sublimation temperatures (measured by two-color pyrometry) of soot particles, which were synthesized in ethylene/air, acetylene/air, and propylene/air flames, plotted against their mean size measured in the statistical processing of low-resolution TEM photomicrographs. Similar data from [9] obtained in a flat premixed ethylene/air flame with the use of a similar burner (but with a different fuel/oxidizer ratio) are also shown in Fig. 7 for comparison. The fuel/oxidizer ratio excess over the stoichiometric ratio in [9] was 2.1, while the corresponding value for the ethylene/air flame in the present study is 2.34. It should be noted that the sublimation temperatures of soot particles in [9] were studied in relation to the height above the burner face, and their mean sizes were determined by TEM. The result of measurement of the sublimation temperature of soot particles with a mean size of 33 nm synthesized in a standard diffusion ethylene flame [31] is also presented in Fig. 7. It can be seen from Fig. 7 that the sublimation temperature of soot particles increases considerably from 2500 to 4500 K as their size increases from 8 to 20 nm. It was difficult to identify particles smaller than 7 nm in size in the studied atmospheric flames of premixed gases using electron microscopy, since particles grow fast to this size within the flame height interval of 1–2 mm, thus precluding one from sampling particles of different sizes. In addition, the number of particles which could be collected on the grid for electron microscopy decreases with their size, making proper statistical processing infeasible.

Soot particles larger than 23 nm in size could not be collected in flat premixed flames, since the process of soot formation ceases after the installation of a flame stabilizer that ensures uniformity of parameters of the flame over its height. Such stabilizers are normally installed at a height of 10–30 mm. Soot particles in diffusion flames grow to large sizes due to the lack of a body limiting the flame

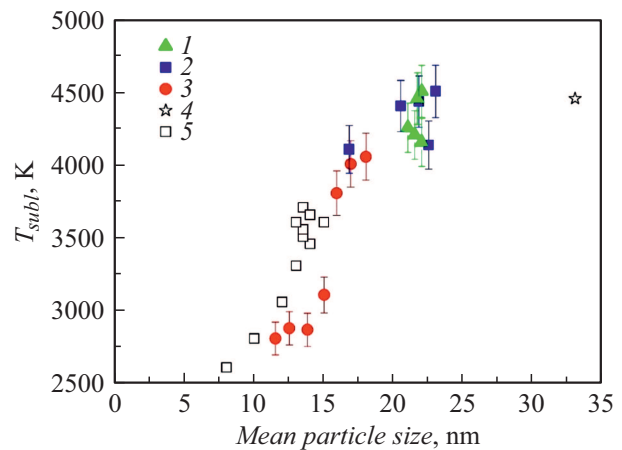


Figure 7. Sublimation temperature of soot particles synthesized in different flames plotted against their mean size: 1 — premixed propylene/air flame (this study), 2 — premixed ethylene/air flame (this study), 3 — premixed acetylene/air flame (this study), 4 — diffusion laminar ethylene flame [31], and 5 — premixed ethylene/air flame [9].

height. Thus, the sublimation temperature of soot particles first increases quickly within the size interval of 8–20 nm and then stabilizes at 4250–4450 K. This may be attributed to the fact that the internal structure of soot particles and, consequently, its thermophysical properties cease to change upon reaching a size of approximately 20 nm. At the same time, it is fair to assume that the thermodynamic and optical properties of soot particles vary considerably within the size interval of 8–20 nm. Note that the sizes of particles in the propylene/air flame fall within the 20–22 nm interval. This is due to the fact that the boundary between the sootless (blue) and sooting (yellow) regions in this flame is very sharp, the amplitude of LII signals increases quickly there, and the signal-to-noise ratio at heights where the particles size is below 20 nm precludes one from conducting proper measurements of the sublimation temperature.

It is worth noting that the temperature differed considerably in the studied flames. This temperature within

the studied interval of heights above the burner face was 1800–1960, 1350–1600, and 950–1000 K in acetylene/air, ethylene/air, and propylene/air flames, respectively. The difference in structure of soot particles formed in a premixed methane/air flame at temperatures of 1650 and 1770 K was examined in [32]. It was demonstrated that the variation of structure of soot particles forming in a premixed flame depends more on the fuel characteristics than on the flame temperature [26,32]. In the present study, the examination of the structure of soot particles synthesized in flames of different hydrocarbons at different temperatures revealed that the correlation with the particle size was stronger than the one with the fuel type and the flame temperature. Thus, although different flame parameters and hydrocarbon types were used in the synthesis of soot particles, we managed to determine the dependence of the sublimation temperature of these particles on their mean sizes without regard to the height in a flame.

As was already noted, the thermodynamic properties of soot particles should be correlated with changes in their internal structure [27]. Using the data obtained by analyzing the structure of soot particles at different stages of their growth in flames, one may identify the correlation between the particle structure and the sublimation temperature. The following structure parameters of soot particles were determined for all the studied flame types and heights above the burner face in statistical processing of the images of samples: mean length and curvature of graphene planes and mean distance between parallel graphene planes. Dependences of these parameters on the mean size of soot particles were plotted. It was found that the mean length of graphene planes of the studied soot particles is on the order of 1.2 ± 0.1 nm and is almost independent of their mean size. The measurement results demonstrate an insignificant reduction in the mean curvature of graphene planes (from 1.4 to 1.3) corresponding to the growth of soot particles within the 10–25 nm interval. Such a minor change in the curvature of graphene planes in the structure of soot particles is unlikely to have caused the observed variation of the sublimation temperature.

The last examined parameter of the structure of soot particles is the mean distance between parallel graphene planes that make up the regions of crystalline structure inside a particle (indicated in Fig. 6). The mean interplanar distances are plotted in Fig. 8 against the mean size of soot particles synthesized in the present study in combustion of propylene, ethylene, and acetylene. It follows from Fig. 8 that the interplanar distance tends to decrease considerably from 0.5 nm to 0.35 nm (a value close to the interplanar distance in graphite, 0.335 nm) as the mean size of soot particles increases from 10 to 25 nm. Thus, of all the studied structure parameters of soot particles, the interplanar distance is the one that is correlated with the behavior of the sublimation temperature in the corresponding interval of particle sizes. It can be concluded that the sublimation temperature of soot particles increases from 2500 to 4500 K as the mean distance between parallel graphene planes

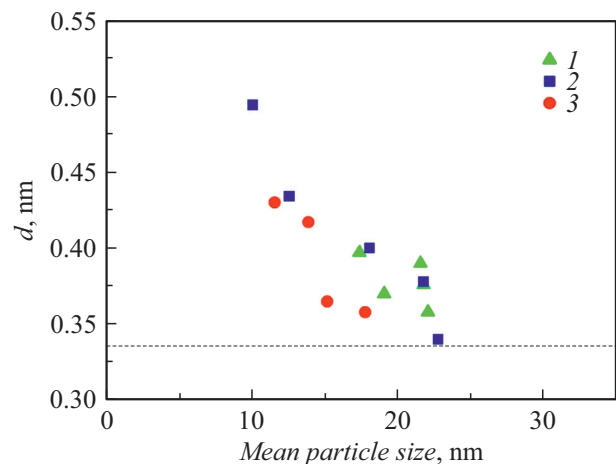


Figure 8. Mean distance between graphene planes in soot particles plotted against the mean particle size. Soot particles were synthesized in: 1 — propylene/air flame, 2 — ethylene/air flame, 3 — acetylene/air flame.

in their structure decreases. In addition, high-resolution photomicrographs reveal that an increase in the mean size of soot particles is accompanied by an increase in both the number of crystallites in the structure of particles and the number of parallel graphene planes in them. At the initial stages of growth of soot particles (with their minimum mean sizes up to 10–12 nm), it is uncommon to find more than two parallel graphene planes in the structure. The number of such paired planes in „young“ particles is also small. Thus, a „young“ soot particle may be characterized as an object with an amorphous structure. As soot particles grow to a mean size of 20 nm and above, the number of parallel graphene planes in a single crystallite increases to 5 or more, and crystalline regions occupy an increasing fraction of the particle volume. As a result, crystalline structures occupy up to 50% of the skeletonized image area. The reduction in the mean interplanar distance is correlated qualitatively with the increase in both the number of graphene planes in a crystallite and the number of crystallites themselves that occurs as soot particles evolve from „young“ to „mature“ ones.

It should be noted that the equilibrium sublimation temperature of graphite at atmospheric pressure is 3900–4000 K [33], and C_3 clusters are predominant in the vapor composition in this case [34]. The maximum temperature of laser sublimation of soot particles measured in the present study (4250–4450 K) is higher than the equilibrium sublimation temperature of C_3 clusters and agrees well with the data on equilibrium sublimation of C_2 clusters (4457 K) [35]. These data suggest that a reduction in the sublimation temperature reflects the process of growth of carbon clusters detached from soot particles as a result of sublimation. This, in turn, is related to the weakening of bonds in the internal structure (due to an increase in the interplanar distance) and a reduction in the

number and size of crystallites that characterize the process of graphitization of growing soot particles. Therefore, the variation of thermodynamic properties of soot depends directly on the degree of graphitization of soot particles. On the other hand, the „older“ a soot particle, the denser its structure and the harder it is to sublime it (the sublimation temperature is higher).

Conclusion

The sublimation temperature of soot particles was determined in accordance with the two-color pyrometry technique by measuring the maximum temperature of laser-heated soot particles with a varying laser energy density. The error of measurement of the maximum laser heating temperature was $\pm 4\%$. The mean sizes of soot particles and the parameters of their structure were studied using a transmission electron microscope. The sublimation temperatures and the mean sizes of soot particles synthesized in ethylene/air ($C/O = 0.78$), acetylene/air ($C/O = 0.72$), and propylene/air ($C/O = 0.9$) flames were determined. Data on the dependence of sublimation temperatures of soot particles formed in premixed flames on their mean sizes were obtained for the first time. In the ethylene/air flame, the sublimation temperatures of soot particles increased from 4100 to 4500 K as their mean size grew from 17 to 22 nm. In the acetylene/air flame, the sublimation temperatures of soot particles increased from 2800 to 4100 K as their mean size grew from 12 to 19 nm. In the propylene/air flame, the sublimation temperatures of soot particles remained within the interval from 4100 to 4500 K at a mean size of 20–22 nm. These results demonstrate that soot particles may be divided into two groups according to their formation stage: „young“ particles with a sublimation temperature of 2800–3200 K and „mature“ particles with a sublimation temperature of 3800–4500 K. These groups have a sharp boundary within the interval of mean sizes from 15 to 17 nm. The observed increase in the sublimation temperatures of soot particles with larger mean sizes is correlated with a reduction in the interplanar distance between parallel graphene planes from 0.5 to 0.35 nm and an increase in the number of parallel planes located close to each other and the number of such crystallites in the particle structure.

Acknowledgments

This study was supported by the Russian Science Foundation, grant No. 19-79-10204.

Conflict of interest

The authors declare that they have no conflict of interest.

References

- [1] T. Ishiguro, Y. Takatori, R. Akihama. *Combust. Flame*, **108**, 231 (1997). DOI: 10.16/S0010-2180(96)00206-4
- [2] V. Fernandez-Alos, J.K. Watson, R. Vander Wal, J.P. Mathews. *Combust. Flame*, **158**, 1807 (2011). DOI: 10.1016/j.combustflame.2011.01.003
- [3] B.S. Haynes, H.Gg. Wagner. *Prog. Energy Combust. Sci.*, **7**, 229 (1981). DOI: 10.1016/0360-1285(81)90001-0
- [4] H. Wang. *Proc. Combust. Inst.*, **33**, 41 (2011). DOI: 10.1016/j.proci.2010.09.009
- [5] P. Desgroux, X. Mercier, K.A. Thomson. *Proc. Combust. Inst.*, **34**, 1713 (2013). DOI: 10.1016/j.proci.2012.09.004
- [6] M. Frenklach. *Phys. Chem. Chem. Phys.*, **4**, 2028 (2002). DOI: 10.1039/B110045A
- [7] L.A. Sgro, A.C. Barone, M. Commodo, A. D'Alessio, A. De Filippo, G. Lanzaolo, P. Minutolo. *Proc. Combust. Inst.*, **32**, 689 (2009). DOI: 10.1016/j.proci.2008.06.216
- [8] M.L. Botero, Y. Sheng, J. Akroyd, J. Martin, J.A.H. Dreyer, W. Yang, M. Kraft. *Carbon*, **141**, 635 (2019). DOI: 10.1016/j.carbon.2018.09.063
- [9] H. Bladh, J. Johnsson, N.-E. Olofsson, A. Bohlin, P.-E. Bengtsson. *Proc. Combust. Inst.*, **33**, 641 (2011). DOI: 10.1016/j.proci.2010.06.166
- [10] S. Bejaoui, S. Batut, F. Therssen, N. Lamoureux, P. Desgroux, F. Liu. *Appl. Phys. B*, **118**, 449 (2015). DOI: 10.1007/s00340-015-6014-3
- [11] A.V. Eremin, E.V. Gurentsov, R.N. Kolotushkin. *Appl. Phys. B*, **126**, 125 (2020). DOI: 10.1007/s00340-020-07426-3
- [12] A.V. Drakon, A.V. Eremin, E.V. Gurentsov, E.Yu. Mikheyeva, R.N. Kolotushkin. *Appl. Phys. B*, **127**, 81 (2021). DOI: 10.1007/s00340-021-07623-8
- [13] E.V. Gurentsov, A.V. Eremin, E.Yu. Mikheyeva. *High Temperature*, **55** (5), 723 (2017). DOI: 10.1134/S0018151X17040071
- [14] K.K. Nanda, A. Maisels, F.E. Kruijs, H. Fissan, S. Stappert. *Phys. Rev. Lett.*, **91**, 106102 (2003). DOI: 10.1103/PhysRevLett.91.106102
- [15] S. De Iuliis, F. Migliorini, F. Cignoli, G. Zizak. *Appl. Phys. B*, **83**, 397 (2006). DOI: 10.1007/s00340-006-2210-5
- [16] D.R. Snelling, F. Liu, G.J. Smallwood, Ö.L. Gülder. *Combust. Flame*, **136**, 180 (2004). DOI: 10.1016/j.combustflame.2003.09.013
- [17] A. Eremin, E. Gurentsov, E. Mikheyeva, K. Priemchenko. *Appl. Phys. B*, **112**, 421 (2013). DOI: 10.1007/s00340-013-5530-2
- [18] E.V. Gurentsov, A.V. Eremin, S.A. Musikhin. *Tech. Phys.* **64**, 1133 (2019). DOI: 10.1134/S1063784219080085
- [19] E. Gurentsov. *Nanotechnol. Rev.*, **7** (6) 583 (2018). DOI: 10.1515/ntrev-2018-0080
- [20] C. Jager, Th. Henning, R. Schlogl, O. Spillecke. *J. Non-Crystall. Sol.*, **258**, 161 (1999). DOI: 10.1016/S0022-3093(99)00436-6
- [21] V. Fernandez-Alos, J.K. Watson, R. Vander Wal, J.P. Mathews. *Combust. Flame*, **158**, 1807 (2011). DOI: 10.1016/j.combustflame.2011.01.003
- [22] C.S. McEnally, Ü.Ö. Köylü, L.D. Pfefferle, D.E. Rosner. *Combust. Flame*, **109**, 701 (1997). DOI: 10.1016/S0010-2180(97)00054-0
- [23] B. Kock, C. Kayan, J. Knipping, H.R. Ortner, P. Roth. *Proc. Combust. Inst.*, **30**, 1689 (2004). DOI: 10.1016/j.proci.2004.07.034
- [24] H.A. Michelsen. *J. Chem. Phys.*, **118**, 7012 (2003). DOI: 10.1063/1.1559483

- [25] X. López-Yglesias, P.E. Schrader, H.A. Michelsen. *J. Aerosol Sci.*, **75**, 43 (2014). DOI: 10.1016/j.jaerosci.2014.04.011
- [26] M. Alfe, B. Apicella, R. Barbella, J.N. Rouzaud, A. Tregrossi, A. Ciajolo. *Proc. Combust. Inst.*, **32**, 697 (2009). DOI: 10.1016/j.proci.2008.06.193
- [27] H.A. Michelsen. *Proc. Combust. Inst.*, **38**, 1197 (2021). DOI: 10.1016/j.proci.2020.06.383
- [28] B. Apicella, P. Pré, J.N. Rouzaud, J. Abrahamson, R.L. Vander Wal, A. Ciajolo, A. Tregrossi, C. Russo. *Combust. Flame*, **204**, 13 (2019). DOI: 10.1016/j.combustflame.2019.02.026
- [29] H.-S. Shim, R.H. Hurt, N.Y.C. Yang. *Carbon*, **38**, 29 (2000). DOI: 10.1016/S0008-6223(99)00096-2
- [30] A. Galvez, N. Herlin-Boime, C. Reynaud, C. Clinard, J.-N. Rouzaud. *Carbon*, **40**, 2775 (2002). DOI: 10.1016/S0008-6223(02)00195-1
- [31] F. Goulay, P.E. Schrader, X. Lopez-Yglesias, H.A. Michelsen. *Appl. Phys. B*, **112**, 287 (2013). DOI: 10.1007/s00340-013-5504-4
- [32] M. Alfe, B. Apicella, J.-N. Rouzaud, A. Tregrossi, A. Ciajolo. *Combust. Flame*, **157**, 1959 (2010). DOI: 10.1016/j.combustflame.2010.02.007
- [33] J. Abrahamson. *Carbon*, **12**, 111 (1974). DOI: 10.1016/0008-6223(74)90019-0
- [34] H.R. Leider, O.H. Krikorian, D.A. Young. *Carbon*, **11**, 555 (1973). DOI: 10.1016/0008-6223(73)90316-3
- [35] H.A. Michelsen, F. Liu, B.F. Kock, H. Bladh, A. Boiarciuc, M. Charwath, T. Dreier, R. Hadeif, M. Hofmann, J. Reimann, S. Will, P.-E. Bengtsson, H. Bockhorn, F. Foucher, K.P. Geigle, C. Mounaim-Rousselle, C. Schulz, R. Stirn, B. Tribalet, R. Suntz. *Appl. Phys. B*, **87**, 503 (2007). DOI: 10.1007/s00340-007-2619-5